2.14 Nuclear Assessment

Radiation transport calculations are very important in an assessment of the ITER design, particularly with regard to operational constraints, access for reactor maintenance and unscheduled repairs, and activated waste (see 5). These calculations are carried out in a progression which begins with 1D studies for scoping, that take into account the reactor operating conditions, followed by 2 and 3D calculations that take into account streaming through penetrations, as well as the complexity of the geometry and the different material thicknesses and compositions.

An accurate map of the radiation fields is necessary all around the system. Component design and disposition of shielding must be decided to meet the objective of getting dose levels within imposed limits on surrounding systems, e.g. magnets, or to ensure personnel safety during operation and after shutdown if access is required for maintenance activities.

The shielding efficiency of the blanket plus the vacuum vessel should satisfy limits which include, for example, the total nuclear heating in the magnet (~14kW), the helium production in the vacuum vessel at points where rewelding may be necessary (~1 appm), and the dose rate after shutdown in areas requiring access (< 100 μSv/h), etc.

For radiation transport calculations, mainly two types of models have been used: 1) 1 and 2D models for deterministic transport codes (ANISN, DANTSYS) and 2) 3D models using a Monte Carlo transport code (MCNP[1]). The 1D method is used to identify ranges of nuclear responses and provide initial design guidance. 3D models have been used to give specific nuclear responses in complex geometries that are more representative of the actual ITER systems.

[1] MCNP 4B, Monte Carlo N-Particle Transport System. Los Alamos National Laboratory, Los Alamos, New Mexico. Ed. by J. Briesmeister, LA-12625-M, Nov. 1993.

The 1D model shown in Figure 2.14-1 is a "toroidal" cylindrical representation of the radial build-up of ITER at the equatorial plane. Such configurations simultaneously include the inboard and the outboard parts of the reactor with the main machine vertical axis as the axis of symmetry.

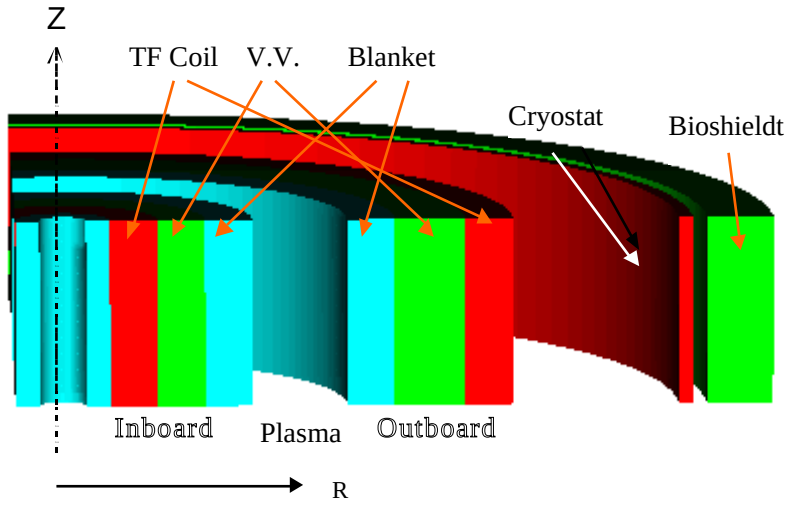

Figure 2.14-1 One Dimensional "Toroidal" Model

For more accurate prediction of the nuclear responses, a fully detailed 3D MCNP model, with 20˚ symmetry, has been constructed. This includes (Figure 2.14-2) a careful representation of the poloidal and toroidal segmentation of the blanket modules, divertor cassettes, vacuum vessel, TF coil, intercoil structure, and cryostat envelope. A few details (which may have some effect on the results) have been neglected, for example, the cooling channel in the blanket modules and heterogeneity of the vacuum vessel (including the flexible joints). A source routine has been written so that the neutron distribution probability emission is very close to the real one, using a matrix whose elements are proportional to the fusion power.

The 3D model with 20˚ symmetry is the basis of all analyses for ITER. For detailed analyses around the ports, modifications have been introduced in the basic model to insert details relevant to the specific study. For the NB injection port analysis, for instance, the standard model has been expanded to 80° to take into account the relevant toroidal asymmetry, and the two tangential neutral beam lines have been modelled in full detail (see 2.14.4).

The following sections range across the whole machine, presenting a summary of the means by which the analyses have been performed, and the main results.

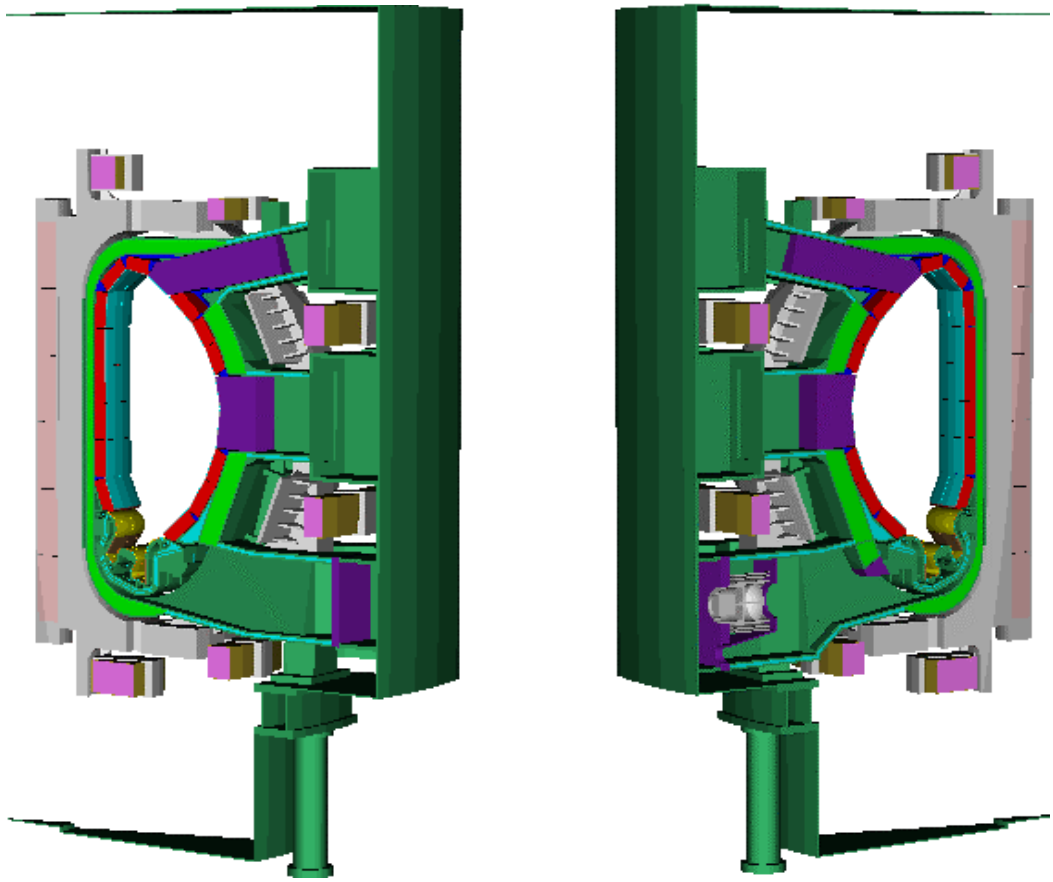

Figure 2.14-2 Outboard View of the ITER Standard Model for the Monte Carlo Calculations showing Different Lower Port Geometry (a) At the Mid-plane of a Divertor RH Port and (b) At the Mid-plane of a Pumping Port

2.14.1 Neutron Wall Loading Distribution on the First Wall

The neutron wall loading (the 14.1-MeV neutron current through the first wall) is usually used by designers as a normalisation factor for a quick estimate of nuclear responses in different parts of the blanket, vacuum vessel and others structural elements of the reactor. The poloidal distribution of the neutron wall loading is shown in Figure 2.14-3 for design scenario I (P_{fus} = 500 MW).

The neutron wall loading, averaged over the inboard part of the first wall (~ 200 m^2), the outboard part (~ 470 m^2) and the divertor surfaces facing the plasma (~ 60 m^2) is ~ 0.55 MW/m^2 at this level of fusion power. The inboard maximum is about 0.59 MW/m^2, and the outboard one ~ 0.78 MW/m^2.

In the case of the hybrid non-inductive operation (design scenario 3, P_{fus} = 400 MW) with a smaller minor radius and outward shifted plasma, the relative peak value at the outboard equatorial plane is slightly (by ~3%) higher than during the reference inductive operation. However, as the fusion power is lower, the average neutron wall loading is 0.44 MW/m^2, and the maximum inboard and outboard neutron wall loads are ~0.46 and ~0.64 MW/m^2 respectively.

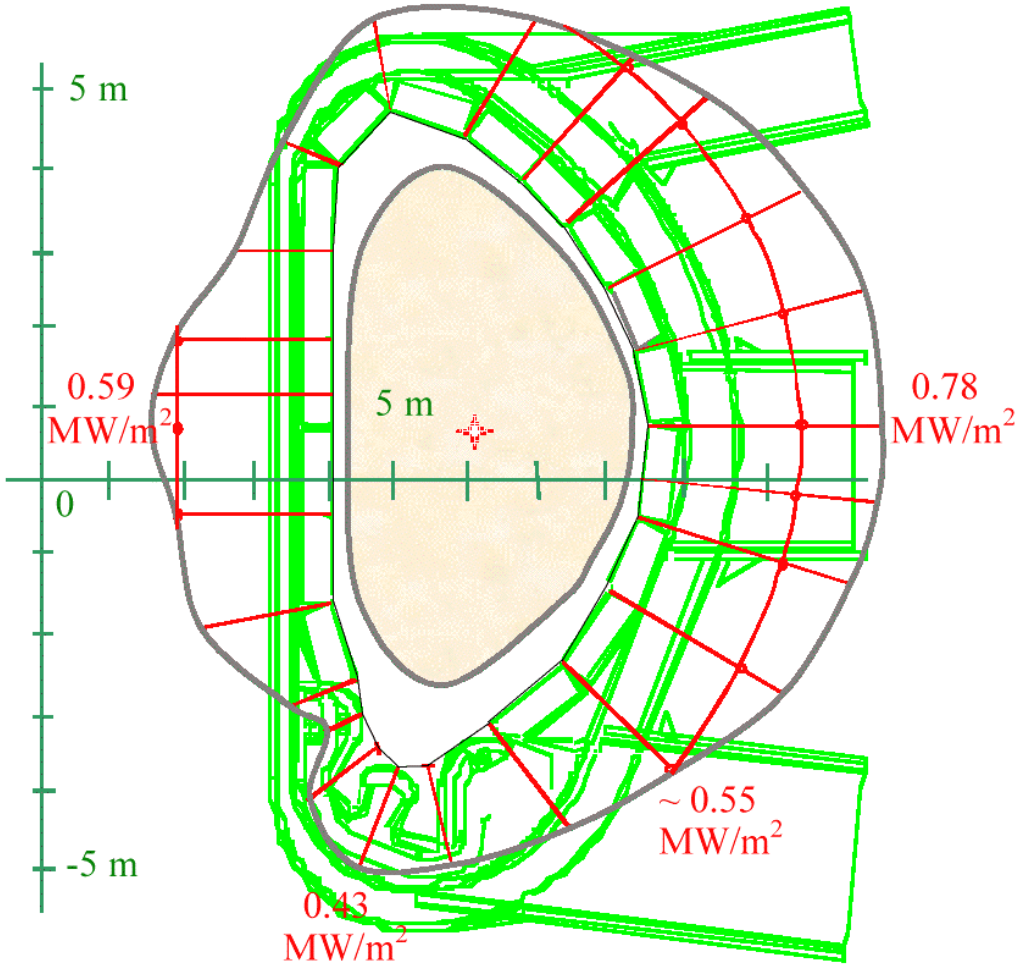

Figure 2.14-3 Poloidal Distribution of the Neutron First Wall Loading (fusion power 500 MW)

2.14.2 Nuclear Power Deposition in the Main Systems

2.14.2.1 Nuclear Energy Multiplication and Total Power

The total power balance in the reactor includes three main components: the fusion power, auxiliary heating, and additional nuclear energy release in the structural components of the reactor.

Under nominal operation, plasma heat radiation (~100 MW) which is ~20% of the fusion power (500 MW), and the auxiliary heating power (P_{heat} = 73 MW), will be deposited in the plasma facing components of the first wall and the divertor.

As a result of the various reactions of neutrons with materials in the blanket, divertor and vacuum vessel structural elements, the total nuclear energy release from both neutrons and secondary photons is about 20 MeV per incident 14.1 MeV source neutron. Table 2.14-1 shows the neutron energy multiplication factors based on 1D and 3D neutron and gamma transport calculations at a nominal fusion power of 500 MW (i.e. 400 MW of 14 MeV neutrons).

Table 2.14-1 Neutron Energy Multiplication by 1D and 3D Transport Calculation

	1D(MW)	3D (MW)
First Wall and Blanket	584	502
Vacuum Vessel	3.6	7.1
Divertor Cassettes	-	49.4
Total	588	559
Neutron energy multiplication factor	1.47	1.40

The 4% difference between two estimates comes mainly from geometric effects (torus versus cylinder) and nuclear data uncertainty. A factor of 1.44 was used as a reference value to avoid underestimating neutron energy multiplication in the blanket.

A more detailed distribution of nuclear energy deposited in each major system of the machine is indicated in the following paragraphs.

2.14.2.2 Heat Deposition in the Blanket Modules

In the standard 3D model, a careful description of the segmentation of the inner vacuum vessel components has been made. Streaming through the poloidal and toroidal gaps between the blanket modules can have a strong impact on nuclear responses in the components behind. There are 17 modules poloidally. The toroidal segmentation is different in the inboard and outboard part: per 20° sector there are 2 outboard modules and 1 inboard.

The overall radial thickness of each blanket module is 45 cm. The radial layout of the module has been modelled with the front beryllium armour (1 cm thick) followed by a 2 cm thick heat sink. The remaining 42 cm is the bulk shield. It has been represented as a homogenised mixture of 84% steel and 16% water.

Other components relevant to the shielding performance have been described in addition. Where used, filler shield elements are inserted in between the blanket modules. Bearing in mind that the blanket coolant manifold is combined with the filler shields, an assumed homogenised material composition of 50% steel and 50% water has been used. The poloidal layout of blanket coolant manifolds has also been included.

The nuclear heating in the blanket system components is summarised in Table 2.14-2

Table 2.14-2 Nuclear Heating in the Blanket Modules (MW)

Inboard first wall	30
Inboard shield module	104
Outboard first wall	59
Outboard shield module	230
Filler wedge elements	7
Manifolds	4
Equatorial port plug	58
Upper port plug	9
Total	502

2.14.2.3 Nuclear Heating in the Divertor Cassette

The divertor cassette has a complex geometry and is made of two kind of components that have different purposes: plasma-facing components for very high heat load removal, and an underlying robust cassette body.

A very detailed model has been made for the divertor. Account has been taken of the heterogeneity and the complicated curvature of the components, the pumping slots and the gap in between the cassette, which affect the streaming through the lower ports. A fine cell subdivision has been made in order to have a detailed poloidal and radial distribution of the nuclear heating. In the 20˚ model one whole cassette and two half cassettes are described to keep the exact symmetry of the system with respect to the port. Table 2.14-3 summarises the heat deposition results.

The analysis refers to an earlier version of the design, whereas the divertor design has since been updated. The update affects mainly the void region under the dome. The cassette itself is not substantially different in thickness and composition. Thus the bulk shielding properties are expected to be the same, as is the average heat production. Some differences are expected in the poloidal distribution of the nuclear responses in the front layers of the plasma-facing components.

Table 2.14-3 Integrated Nuclear Heat Deposition within the Complete Divertor System

Divertor Component	**Heating[MW]**
Outer Target	16.4
Inner Target	7.0
Dome	7.0
Cassette	12.0
Total	49.4

2.14.2.4 Nuclear Heating in the Vacuum Vessel

The vacuum vessel has been modelled according to its layout by three layers. There are two robust shells 6 cm thick, both made of pure SS 316 L(N) IG. The thickness of the filler region between the two shells varies poloidally and has been described as an homogenised material

mixture which was assumed to be borated steel 60% ($2^{w}/_{o}$ of natural boron) and 40% water. The overall thickness of the vacuum vessel at the equator is 33.7 cm at the inboard and 75 cm at the outboard.

Results of analysis are summarised in Table 2.14-4. The maximum power density on the surface of the inner layer of the vacuum vessel is 0.3 W/cm^3. This value takes into account the enhancement due to both poloidal and toroidal gaps in between the modules.

Table 2.14-4 Nuclear Heat Deposition in the Vacuum Vessel (kW)

Inboard Vacuum Vessel	997
Top Vacuum Vessel	819
Outboard Vacuum Vessel	3260
Bottom Vacuum Vessel	324
Triangular Support Structures for Modules	1296
Port Walls	396
Total	7092

2.14.2.5 Nuclear Heating in the Superconducting Magnets System

Minimal nuclear heat deposition in the superconducting coils is one of the strong design requirements. The analysis shows that nuclear heating of the toroidal and poloidal field coils and intercoil structures is mainly due to the neutron and gamma rays leaking through the bulk shield and the vacuum vessel port extensions, with some contribution from ^{16}N-decay gamma rays emitted by the outlet blanket water coolant, activated by DT neutrons in the first wall region.

The estimated total nuclear heating in the TF coils and intercoil structures from neutrons and prompt gamma rays is ~13 kW, depending on the in-port plug shielding efficiency. The main part (~ 10 kW) is deposited in the inner straight TF coil legs (Figure 2.14-4) in front of which the thickness of the shielding blanket and vacuum vessel is smallest (~79 cm).

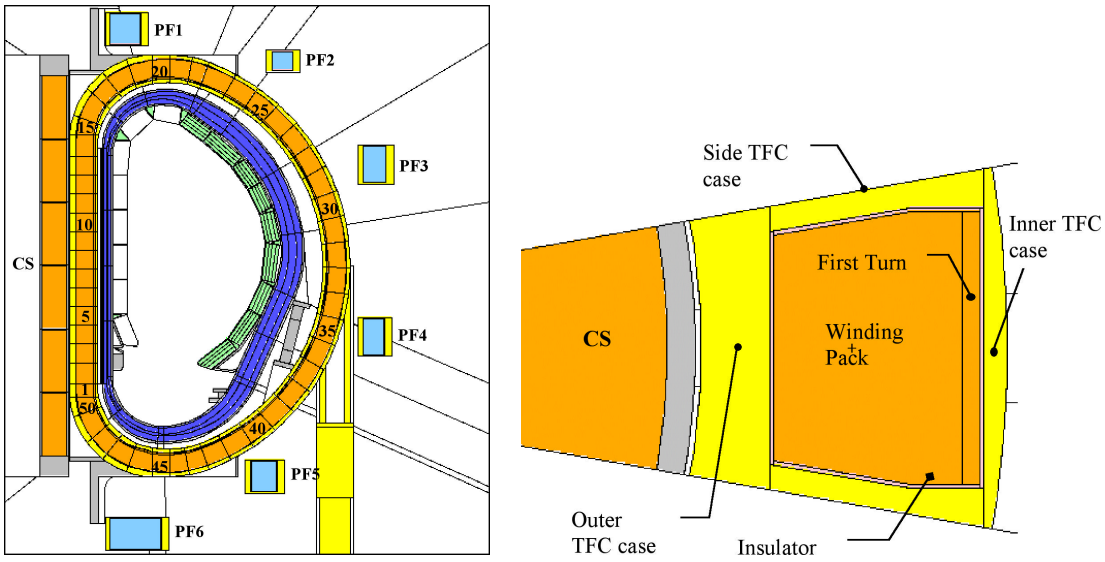

Figure 2.14-4 Superconducting Magnet Model and the Inner TF Coil Leg Cross-section

The specific nuclear heating must also be limited within the local capacity of the He cooling. In the vertical mid-plane of the TF coil legs the local maxima do not exceed ~1 mW/cm^3 and ~0.3 mW/cm^3 in the front steel cases and in the first superconductor layer, respectively. Other magnet nuclear responses, such as the damage to the copper stabiliser, the total insulator dose, and the fast neutron fluence in the first superconductor at the end of the DT operational campaign (at first wall neutron fluence of 0.3 MWa/m^2), are below possible limiting values for these components.

The thickness of the outboard bulk shield is 45-cm (blanket) + ~ 75cm (vacuum vessel) due to the desire to be able to allow hands-on maintenance within the cryostat two weeks after shutdown. Reducing the shutdown dose rates at the maintenance locations requires a factor of one hundred more attenuation than required to reduce the magnet nuclear heating. Thus the nuclear heating of the outer TF coil parts is much lower than the inner TF coil legs.

The total nuclear energy deposition in six poloidal coils varies between 2 W in the upper PF1 and ~ 250 W in PF5 below the divertor port walls (Figure 2.14-4). The total heating rate in all PF coils is < 0.5 kW. The maximum specific nuclear heating in the poloidal field coils is ~ 0.01 mW/cm^3.

The specific ^{16}N-activity in the water coolant in the upper port is ~1.5 x 10^9 Bq/cm^3 or ~ 0.04 Ci/cm^3. The total ^{16}N-decay gamma ray source in the outlet cooling pipes passing through the upper port walls at the cryostat releases ~ 9 kW. The largest fraction of this is released in water itself, in the pipe walls and in the room temperature components inside the cryostat. About 300 W is distributed between different cryogenic components.

The estimated specific nuclear heating in the poloidal field coils and the coil clamps from ^{16}N-decay photons is low, < 0.03 mW/cm^3.

2.14.2.6 Nuclear Heating in the Cryo-pump

A 3D calculation has been carried out to obtain the heating in the cryo-pump system (Figure 2.14-2b). In the 3D standard model, the cryo-pump port has been partially closed by an extension of the vacuum vessel into the port from above. In such a configuration, the overall heat on the pump assembly is 160 W (for one single pump system). Only a small amount (1.8 W) goes to the 4K array, with an average 0.15 mW/cm^3 volumetric power density. A fine subdivision of the 4K array into 12 cells (3 in the radial direction, and 4 in the axial direction) has shown that the peak value is 30% above the average value. If the partial closure at the port entrance were removed, the heating would be 3 times higher.

2.14.2.7 Thermal Shield Nuclear Heating

The vacuum vessel thermal shield (VVTS) is located between the vacuum vessel and the superconducting magnets and covers both inboard (~ 970 m^2) and outboard surfaces (~ 580 m^2) of the vacuum vessel and the port extensions (~ 1030 m^2). A compressed 80K helium gas flow provided by the cryogenic system will be used for an active cooling of the VVTS inside the cryostat.

The heat loads to the VVTS are nearly all by thermal radiation from the room-temperature components. Additional nuclear heat loads are small and are determined mainly by the secondary gamma ray absorption in the steel VVTS structure. The nuclear energy deposition in gaseous helium in the pipes attached to the thermal shield is insignificant.

The specific nuclear heating ~ 2 x 10^{-4} Wcm^{-3} is expected in the innermost part of the thermal shield (~2.2 cm steel) in front of the straight TF coil legs, where the thickness of the bulk radiation shield including the ~ 45 cm blanket and the 34 cm vacuum vessel is minimal.

The specific nuclear energy deposition in the outer ~ 1.8 cm thermal shield behind the 45 cm blanket and thick 75 cm vacuum vessel is ~ 1.0x 10^{-6} Wcm^{-3}. This is much lower than in the inboard part for reasons stated earlier. The main contributors potentially increasing this value locally are the diagnostic and other in-port structures, such as the NB injector.

Additional nuclear heating from the ^{16}N decay gamma source in the outlet water pipes in the locations of the stiff ring that supports the thermal shield and the VVTS-holders is about ~ 2 x 10^{-6} W/cm^3.

The overall nuclear heat load on the VVTS at the nominal fusion power of 500 MW is ~1.7 kW. The largest fraction (~ 69%) is deposited in the inner part of the thermal shield. A further ~ 27% is deposited in the bottom part just below the inner divertor targets. The remaining 3 % is deposited in the vacuum vessel and port coverage (~ 60-90 W), the stiff ring (~ 35-50 W), and the thermal shield holders (~ 3-5 W). The overall nuclear heating of the VVTS appears to be much smaller than other heat loads and does not cause a significant problem for the cryogenic system.

2.14.3 Other Nuclear Responses

2.14.3.1 Damage in the Blanket and Vacuum Vessel Materials

The damage accumulated in materials, and preloading relaxation induced by radiation, is an important design constraint for the development of the separate first wall fasteners and blanket attachments.

Principally, the damage cross sections depend on the material and the neutron spectrum. About 90% of the damage production in metals is determined by fast (E > 0.1 MeV) neutrons. For this reason, the damage production rates are not too sensitive to local non-uniformity in the blanket structure. Their spatial distribution through the blanket depth follows the fast neutron flux distribution.

Figure 2.14-5 shows the radial 1D dpa distributions in the bulk shielding blanket from the first wall to the vacuum vessel ignoring possible local peaking due to the neutron streaming through access holes.

The peaking factor for damage at the bolt end surface does not exceed ~1.3 in comparison with the value in the bulk shield at the same distance (~33 cm) from the first wall. The peaking factor, estimated for the 13 mm hole to access the bimetallic stud at the distance ~70 mm from the first wall inner surface, is about ~1.1.

Figure 2.14-5 compares also the damage accumulated in different materials. The damage in titanium alloys resulting from fusion neutron irradiation is ~10-30 % higher than that in steel. The damage in other materials are nearly the same for the same locations in the blanket depth as that in steel: in Inconel by ~5-15 % higher, in Cu-alloy by ~ 0-10 % higher.

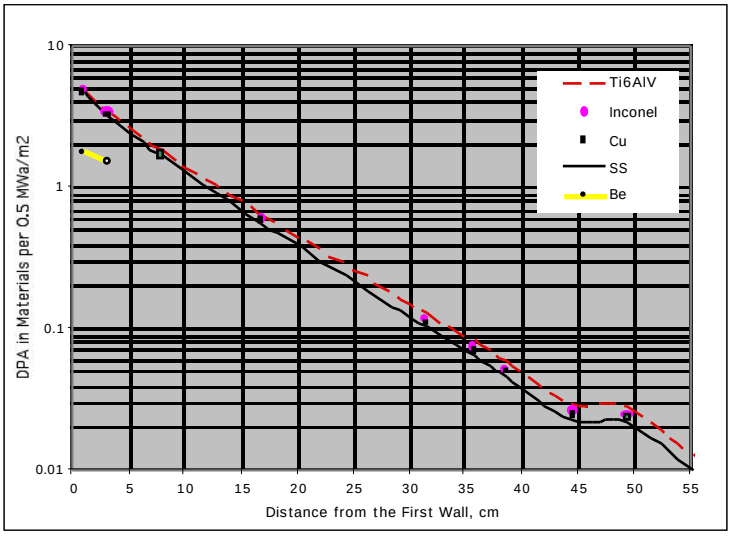

Figure 2.14-5 1D Radial Distributions of Damage in the Blanket and Attachment Materials (Neutron Fluence 0.5 MWa/m^2)

The first wall fastener assemblies (in blanket option A) are located at a distance of ~ 6-15 cm from the inner surface of the plasma chamber and attach the separate first wall panels to the shielding blanket blocks. The damage accumulated in different elements of the first wall

fasteners (such as the threaded bush and bimetallic stud made of Inconel with a copper rod) and calculated in a 2D geometry are shown in Figure 2.14-6.

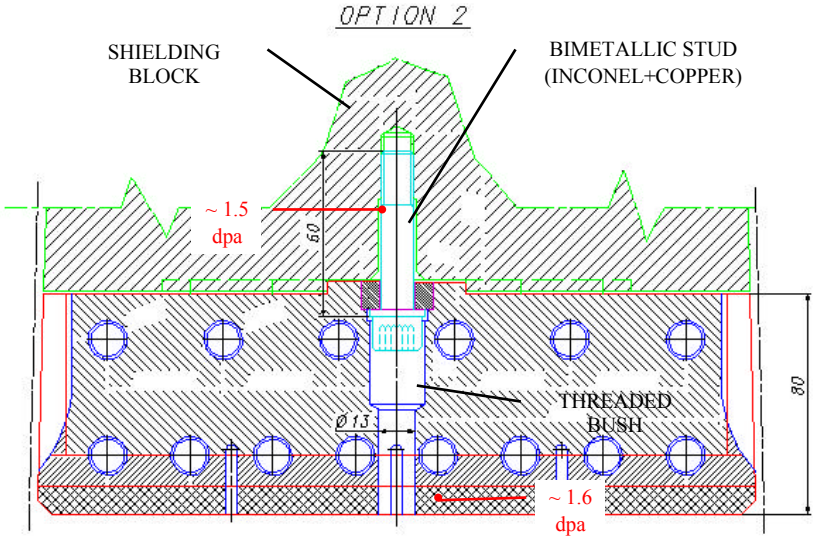

Figure 2.14-6 Damage Expected in Some Elements of the First Wall Fastener (Neutron Fluence 0.5 MWa/m^2)

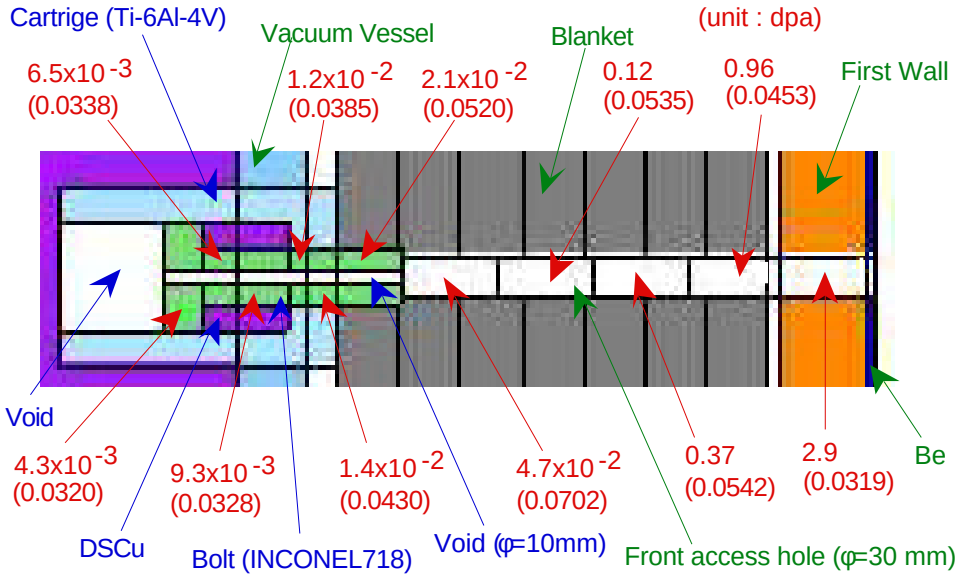

Figure 2.14-7 Damage in Flexible Support Assembly and Surrounding Region (Neutron Fluence 0.5 MWa/m^2)

The maximum damage in the Inconel threaded bush is ~3.4-2.9 dpa on its axis. A factor of two lower values are expected in the lower part of the bolt shank.

The maximum damage in the Inconel bolt end of the blanket attachment system (Figure 2.14-7) is ~ 0.02 dpa.

In the vacuum vessel the damage production attenuates exponentially beginning from ~0.02 dpa in the front steel layer. This “dose” is low and will not result in significant property changes of the structural materials.

All the above values are normalised to the maximum local neutron fluence of 0.5 MWa/m^2, which is the local maximum expected in the outboard first wall at the end of the DT-operation campaign with a nominal average neutron fluence of 0.3 MWa/m^2. The dpa-values and the spatial distributions presented may be used for scaling to other local fluence and bolt positions.

2.14.3.2 He Production

He production in stainless steel is an important parameter for those parts of the vacuum vessel and blanket that need to be rewelded during maintenance or replacement. He-production rates have been estimated for two critical locations where the capability of re-welding is required: the front layer of the outboard vacuum vessel, and the cooling branch pipes in the blanket modules. An average first wall neutron fluence of 0.3 MWa/m^2 is assumed in this analysis.

By 1D calculation, the He-production is estimated to be ~ 0.13 appm at the front part of the vessel, which is made of the SS316L(N)-IG with low boron content (~ 10 wppm). About six times higher values are expected behind gaps (2 cm) between blanket modules, giving ~ 0.8 appm as a local peak value, which is below the limit of 1 appm.

Figure 2.14-8 shows the helium production in the front access hole and branch pipe of the blanket module obtained with the 3D model for the reference structural material, SS316L(N)-IG, which has low boron content (~ 10 wppm). Boron in the steel makes a large contribution to helium production through its large $B^{10}(n,\alpha)$ reaction cross section in the region where thermal neutron flux dominates. The helium production at the welded part of the branch pipe is estimated to be 1.2 dpa.

The design limit of helium production for a re-welded part is 1 dpa for thicker welds. For thinner welds, like that of the branch pipe, the limiting value is now under investigation, but there are indications that higher values can be tolerated. If it is the same as that for thicker welding, branch pipe re-welding could be a serious problem. If higher dpa values are acceptable (for example 3 dpa), re-welding of the branch pipe would be possible.

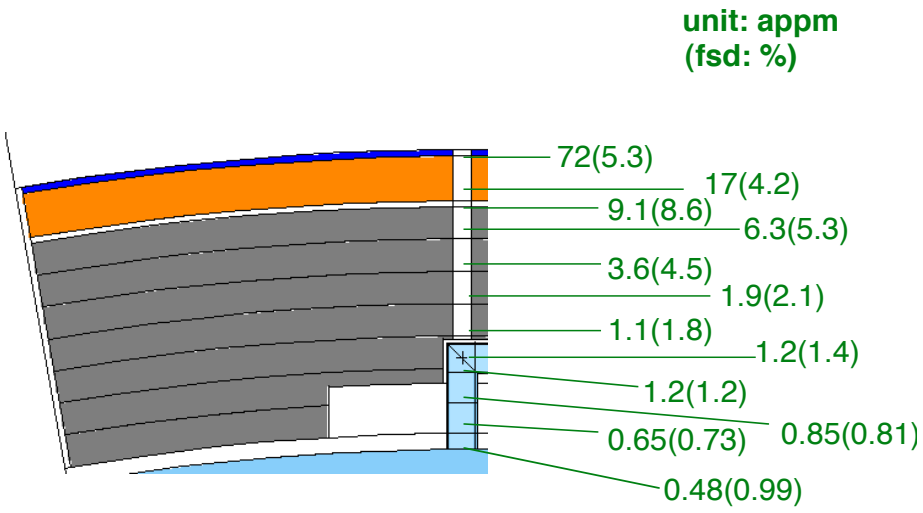

Fig.2.14-8 Helium Production Distribution in SS with 10 wppm B Along the Front Access Hole and the Cooling Water Branch Pipe (Neutron Fluence: 0.3 MWa/m^2)

2.14.4 Dose Rate

In the space inside the cryostat, limited personnel access is envisaged for repair of unexpected defects. At the port locations where personnel should have access for maintenance, the dose rate should be less than 100 μSv/h about 2 weeks (~ 10^6 s) after shutdown. Dose rate behind the bioshield, where more frequent and longer access is necessary, is required to be less than 10 μSv/h.

In order to satisfy these limits, the design relies on the performance of the bulk shielding provided by the outboard blanket and vacuum vessel as well as the bioshield. These alone would bring the dose rate well below the above limits. However the dose rate is dominated, both inside and outside the bioshield, by the presence of numerous penetrations (including NB ports) which are necessary to provide various access routes to the plasma and which affect the shielding capability of both vacuum vessel and bioshield.

The required shielding of these penetrations has been subject to exhaustive dose rate analyses which have been and will be carried out in increasing detail. The main results so far are reported here.

During machine operation, the dose rate around the torus is too high for personnel access. Figure 2.14-9 shows the operation dose rate distribution obtained by a 1D calculation. Although the dose rate behind the bio-shield is shown to be low enough (~1 μSv/h) for personnel access, in practice it is impossible to access there because of radiation streaming through the many penetrations in the bio-shield. (Such access during operation will of course anyway be ruled out by the presence of strongly varying magnetic fields.)

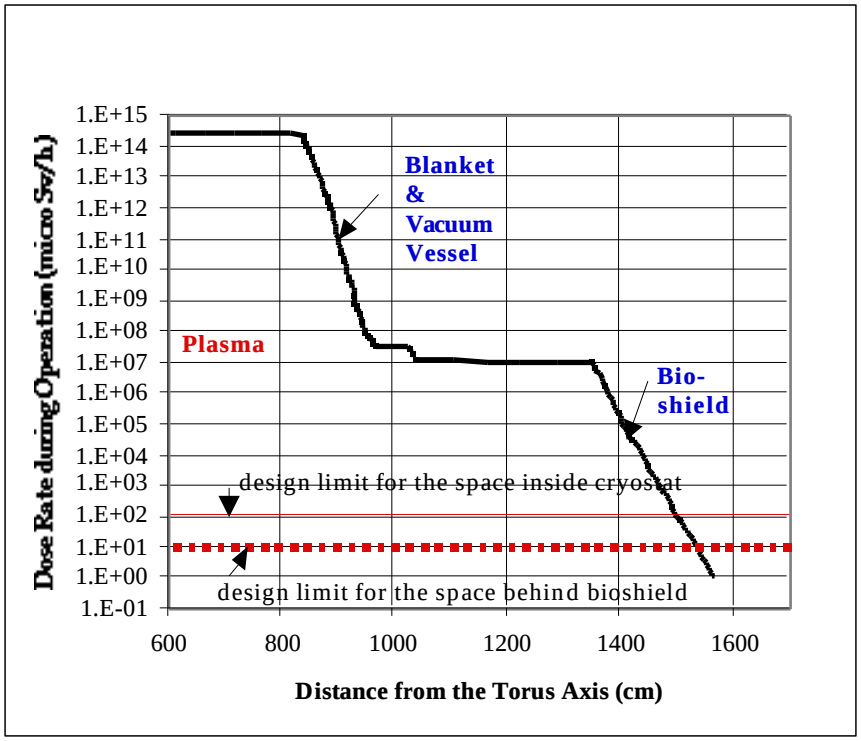

Figure 2.14-9 Dose Rate Distribution During Operation

2.14.4.1 Shutdown Dose Rate Outside Maintenance Port

There are four ports for blanket module maintenance purposes (3, 12, 8 and 17). During operation, plugs are inserted in all of those ports. Two of them have limiters with alignment adjusting mechanisms in their plug. The other two contain diagnostics.

Figures 2.14-10 and -11 show a 3D model of the maintenance port with the limiter. Calculated dose rates due to decay gamma rays around the port 10^6 s after shutdown are shown in Figures 2.14-12(a) and (b). The dose rate levels are generally low in comparison with the design target of 100 μSv/h. This means that there will be no significant problem caused by these ports for personnel access for the preparatory work involved in the removal or re-installation of those plugs.

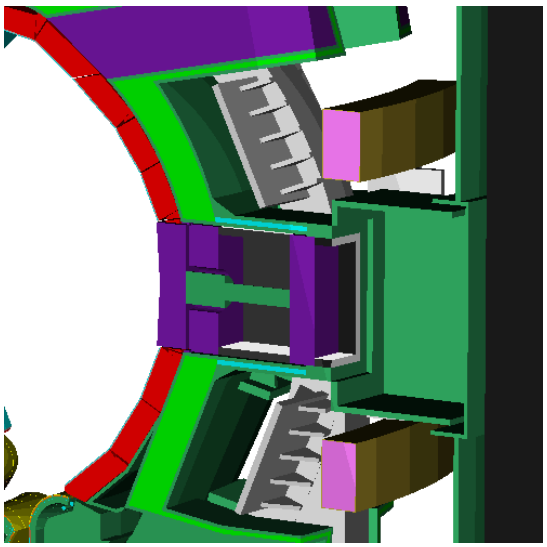

Figure 2.14-10
Limiter Port 3D MCNP Model

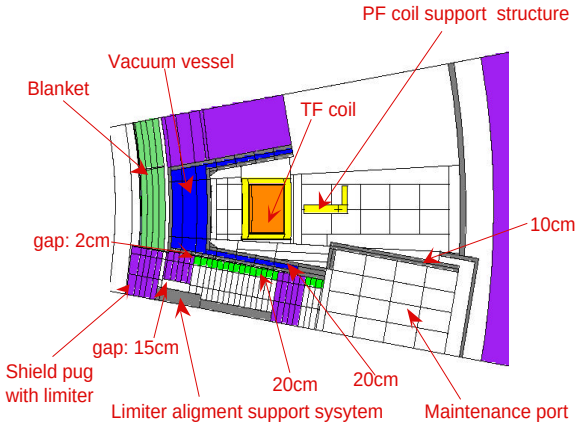

Figure 2.14-11
Horizontal Cross- section of the Limiter Port 3D Model

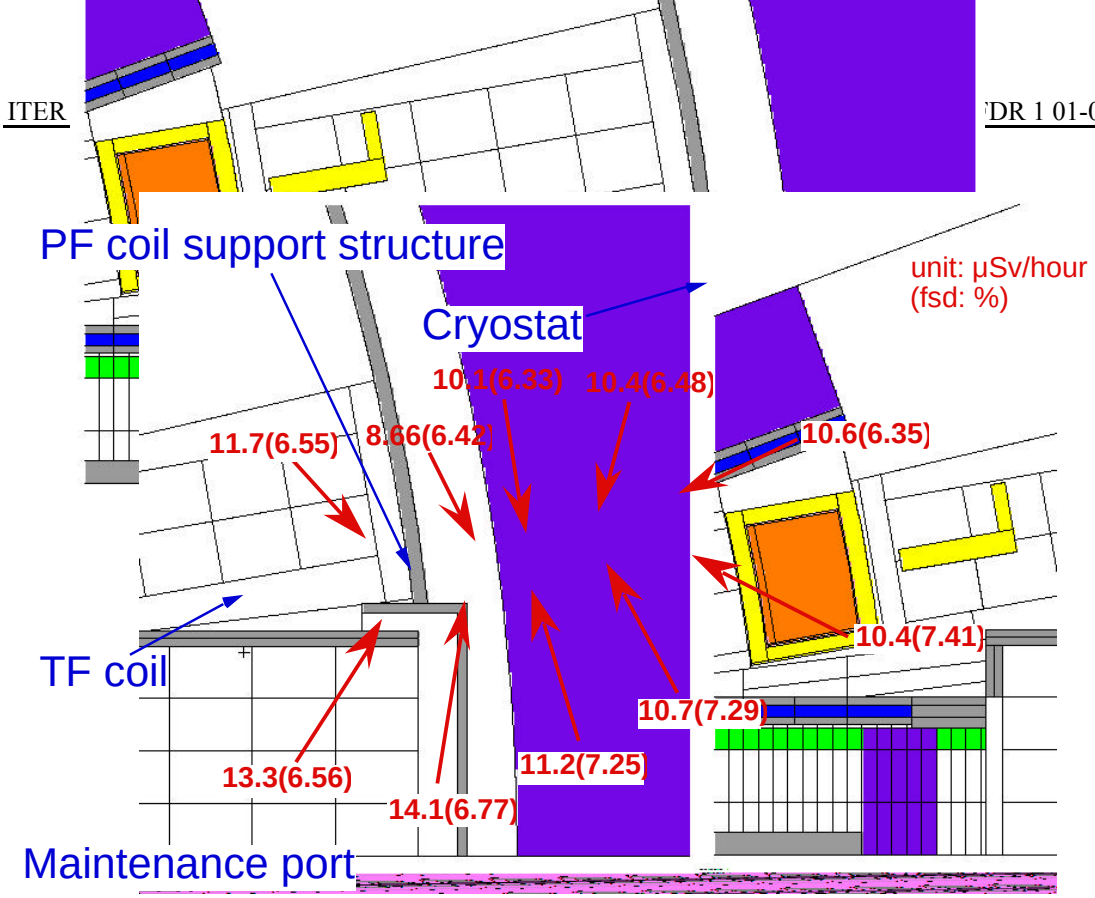

Figure 2.14-12(a) Shutdown Dose Rate Distribution (after 10^6 s)
Outside the Limiter Port
(for average neutron fluence of 0.3 Mwam^{-2})

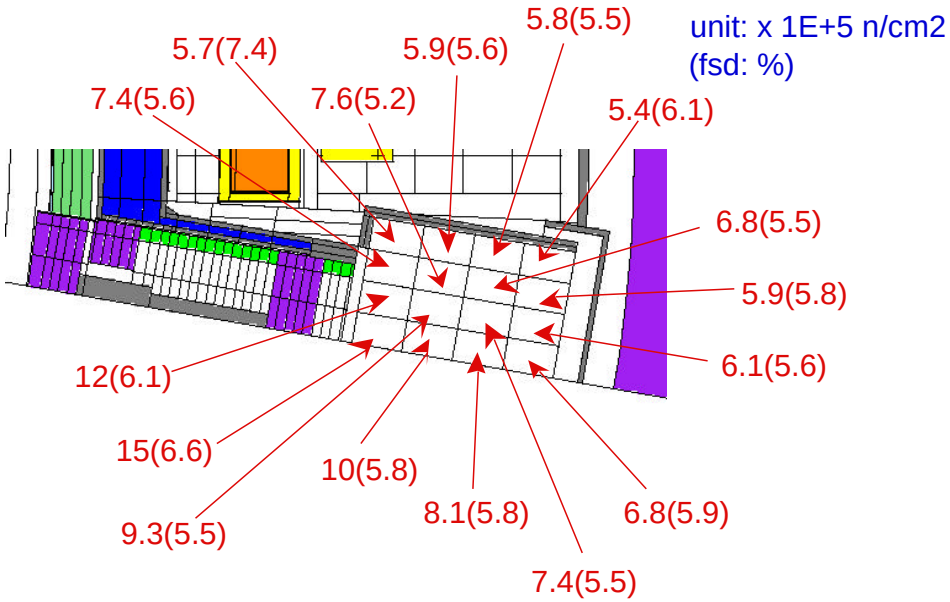

Figure 2.14-12(b) Shutdown Dose Rate Distribution (after 10^6 s)
Inside the Limiter Port
(for average neutron fluence of 0.3 Mwam^{-2})

2.14.4.2 Shutdown Dose Rate Outside NB Injection Port

Equatorial ports 4 and 5 are used for NB injection for plasma heating. A diagnostic NB injector is also installed on port 4. Since the NB lines in these ports are completely open, NB injection ports are a major concern for neutron streaming from the plasma, and a careful shielding design is required.

Previous calculation has shown that a total wall shielding thickness of about 60 cm is enough to provide the required attenuation. However the present design, in order to provide a suitable NB current drive capacity as well as additional strength for the inter-coil structure, provides a local minimum shielding thickness around the NB duct of only about 45 cm. This causes some unacceptable dose rates in the neighbourhood of the duct itself. However this problem is under additional detailed investigation, and it is expected to be solved by providing additional local shielding around the weak point of the port wall.

Figures 2.14-13 and -14 show the 3D Monte Carlo calculation model for the NB injection ports. Calculated dose rates due to decay gamma rays around the port 10^6 s after shutdown are shown in Figure 2.14-15. They are higher than the design limit of 100 μSv/h in some positions and suggest the necessity to avoid access of personnel at these positions (if shielding improvements turn out to be too difficult to achieve).

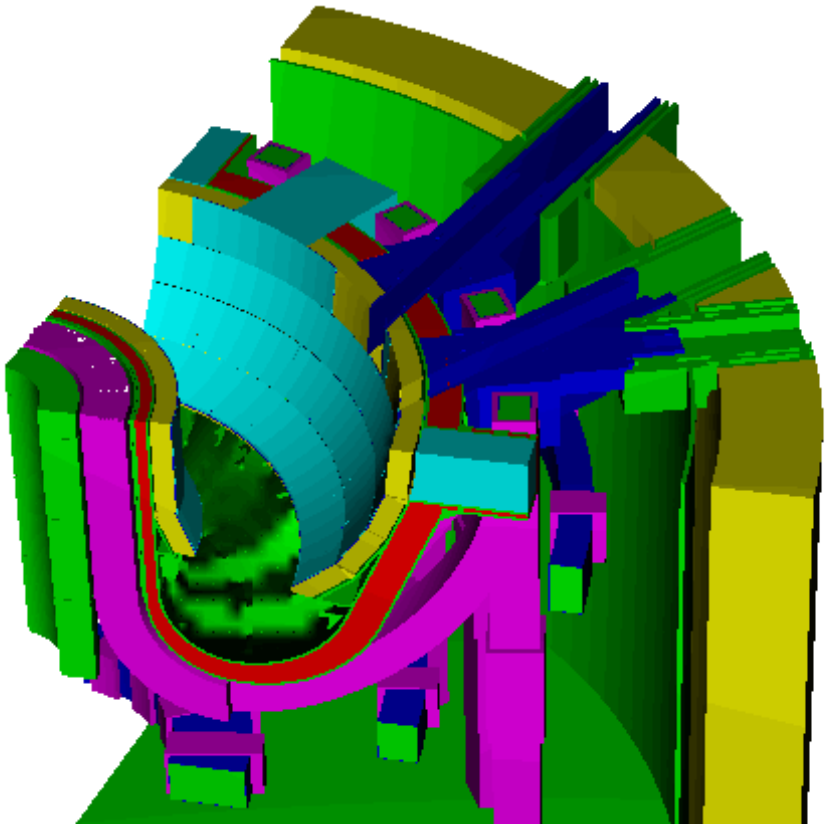

Figure 2.14-13 NB Injection 3D MCNP Model

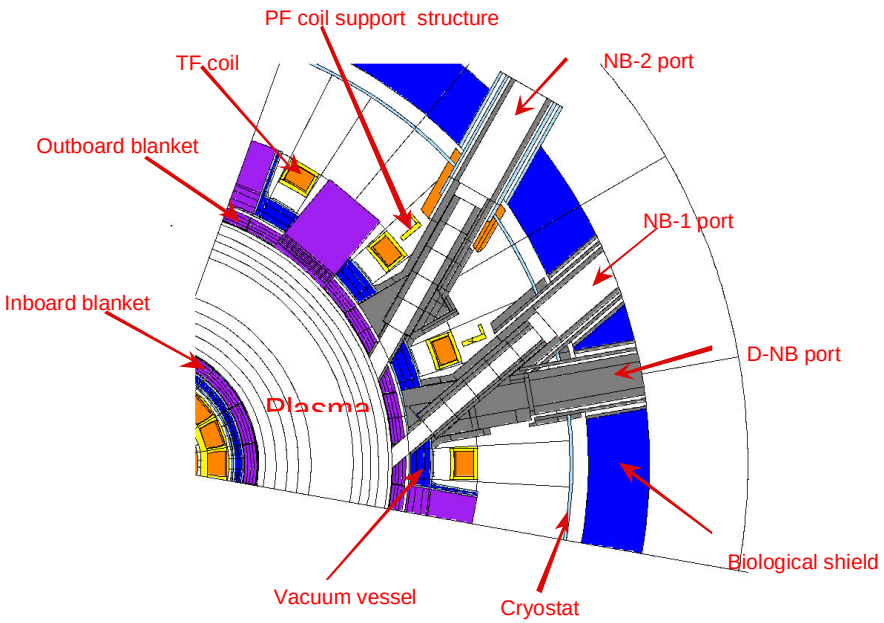

Figure 2.14-14 Horizontal Cross-section of the NBI 3D Model

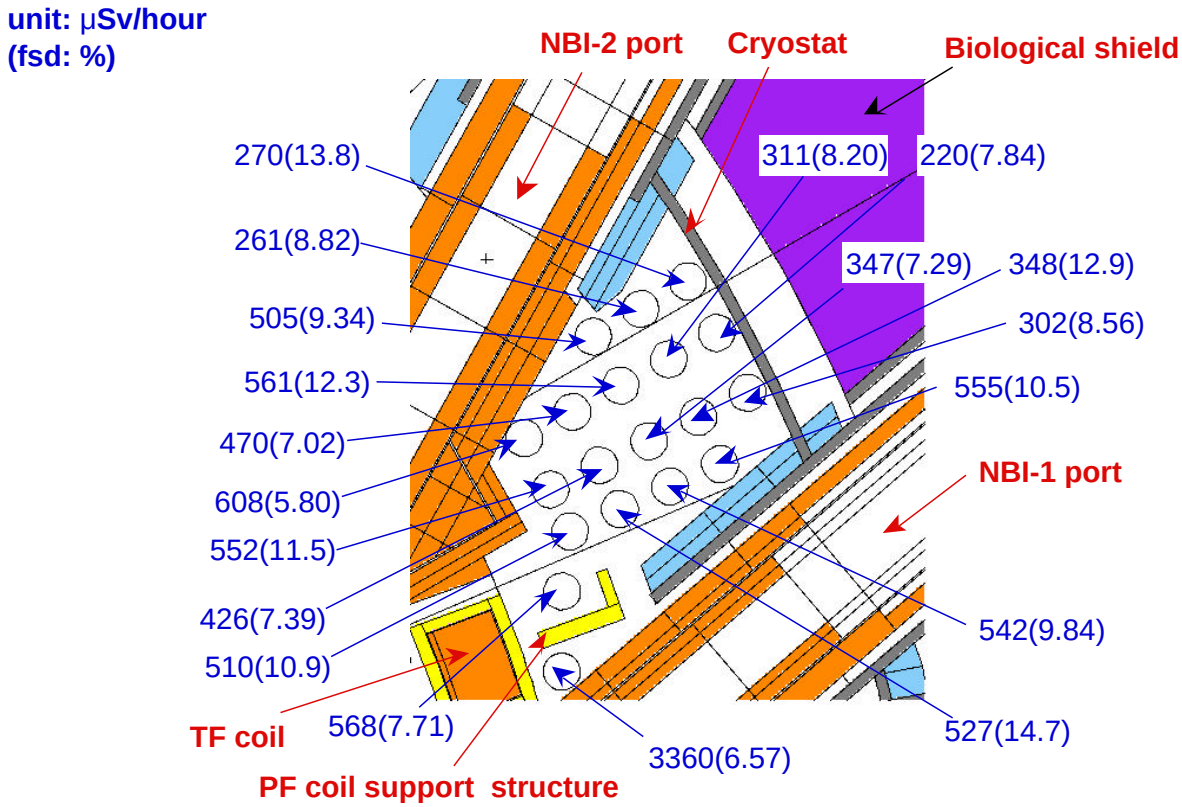

Figure 2.14-15 Shutdown Dose Rate Distribution (10^6 s After Shutdown) Around the NBI Port (for average neutron fluence of 0.3 Mwam^{-2})

2.14.4.3 Divertor Port

The dose rate level around the divertor ports is a problematic issue, mainly as a consequence of the need to have high gas conductance between the divertor plasma region and the cryopump. Dose rates have been calculated using a new methodology, the so-called "one-step" method.

Different shielding configurations have been considered to see the impact on the response functions. The reference port configuration (for all ports except the remote handling ports) foresees (Figure 2.14-16) an extension of the vacuum vessel into the port down to the rail supporting the divertor cassette ("port closed"). This additional shield reduces the poloidal mouth entrance of the port itself, without great impedance increase to the pumps. The in-vessel viewing system (IVV) channel has been considered void in some cases (IVVC open) or closed by a plug (IVVC closed). Values are in Table 2.14-5 and 2. In the table not all the figures are completed for tallying region number 5, but nevertheless it can be seen that a viable solution close to cryostat can be achieved when all the penetrations are reduced. Borated steel added to wall ports can help, removing low energy neutrons from the system.

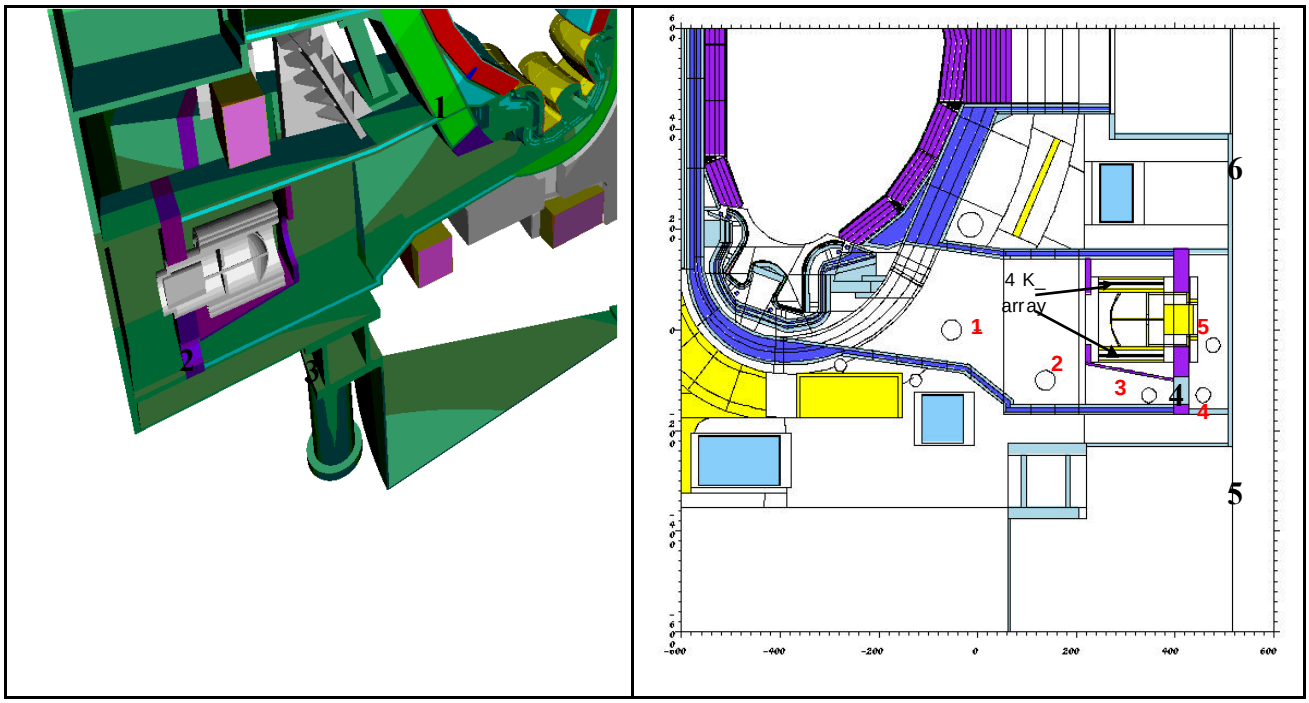

Figure 2.14-16 Section of the Model Cryopump(section AA, left), and Toroidal Section at the Level of the Divertor Region (section BB, right)

Table 2.14-5 Dose Rate Values [μSv/h] Calculated in 5 Positions Inside the CP Port for Different Shielding Configurations.
The last column refers to a configuration with all the penetrations open but with borated steel in the walls covering the walls of the port.

	Open port IVVC open	Open port IVVC closed	Closed port IVVC open	Closed port IVVC closed	Open port IVVC open, borated steel in the walls
1	$7.74\ 10^4$	$8.11\ 10^4$	$6.12\ 10^4$	$5.82\ 10^4$	$7.73\ 10^4$
2	$2.05\ 10^4$	$3.37\ 10^4$	$9.43\ 10^3$	$1.14\ 10^4$	$1.65\ 10^4$
3	1.3310^4	$1.50\ 10^4$	$7.11\ 10^3$	$8.73\ 10^3$	$8.60\ 10^3$
4	$3.21\ 10^3$	$6.78\ 10^2$	$2.77\ 10^3$	$2.27\ 10^2$	$1.07\ 10^3$
5	$9.01\ 10^2$	$7.13\ 10^2$			

2.14.4.4 Shutdown Dose Rate Outside RF H & CD Port

The IC H & CD launcher plug is installed in equatorial ports 13 and 15. While this plug provides rather good bulk shielding, it has been necessary to verify the adequacy of the dogleg in the gap between plug and port wall to avoid excessive neutron streaming. 3D pictures of the model are shown in Figures 2.14-17 and 2.14-18.

The calculated dose rates due to decay gamma rays around the port, 10^6 s after shutdown are shown in Figure 2.14-19. It can be concluded that the shutdown dose rates outside the port are generally below the target of 100 μSv/h.

The EC H&CD launcher plug is installed on the equatorial port 14. Calculated dose rates due to decay gamma rays around the port are similar to those for the IC H&CD port. The EC H&CD system also uses upper ports. Calculations are underway to assess the dose rates.

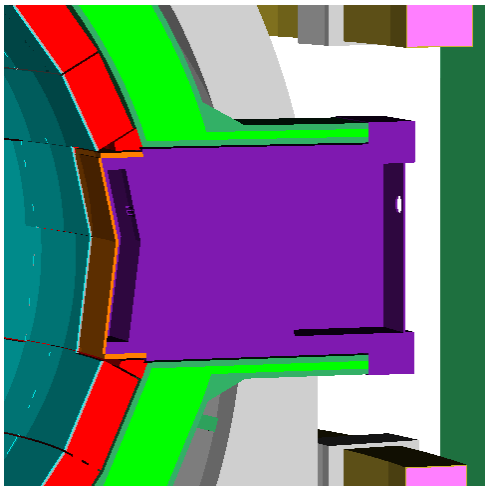

Figure 2.14-17
IC H&CD Port 3D MCNP Model

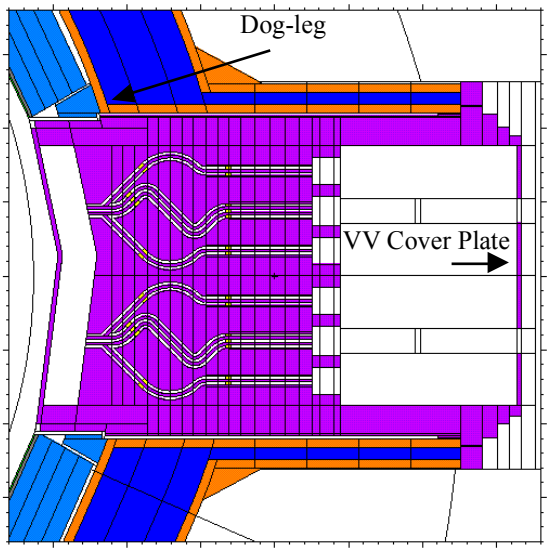

Figure 2.14-18
IC H&CD Port Vertical Cross-section

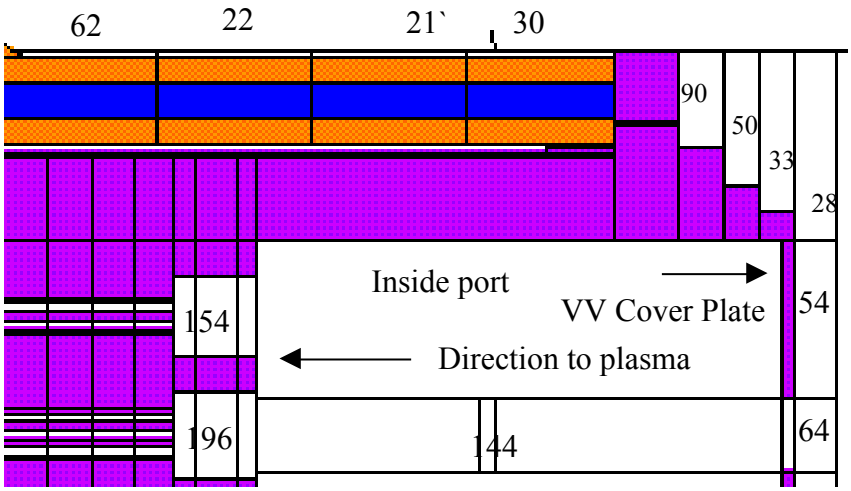

Figure 2.14-19 Dose Rates Around IC H&CD Port in µSv/h 10^6 s After Shutdown

2.14.4.5 Diagnostic Ports

A number of diagnostic plug layouts have been and will be analysed to cover the requirements of all diagnostic systems[1]. Some of them do not alter the bulk shielding efficiency. In other cases, when diagnostic access apertures affect the effective blanket/vacuum vessel shielding capability, this is recovered by labyrinthine access penetrations in special steel/water shielding plugs.

Representative configurations are shown in this section. For example, the 3D model of the edge Thomson scattering system in the upper port is shown in Figure 2.14-20.

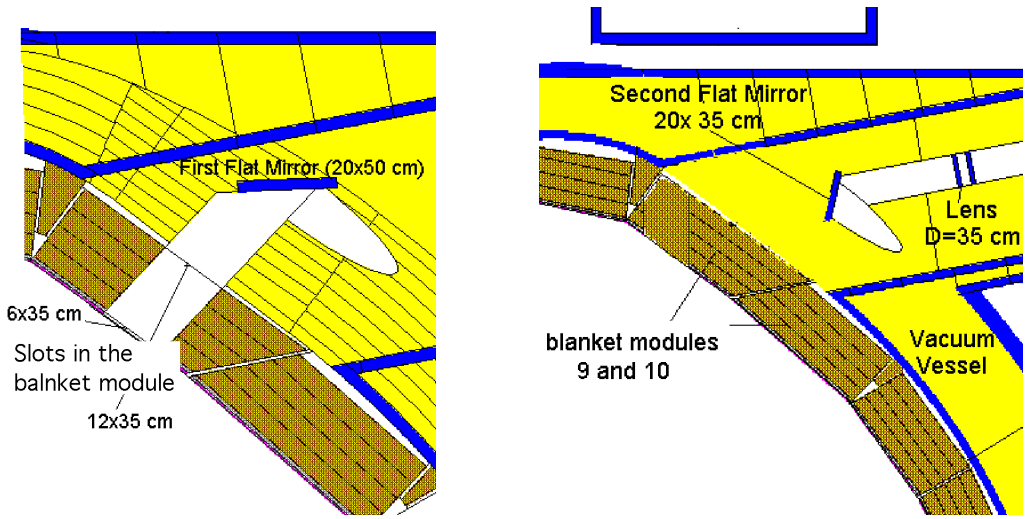

Figure 2.14-20 3D Model of the Edge Thomson Scattering System in the Upper Port

[1] C. I. Walker, S. Yamamoto, A. Costley, L. de Kock, K. Ebisawa, P. Edmonds, G. Janeschitz, V. Khripunov, E. Martin, G. Vayakis. Nuclear Aspects of Diagnostics for RTO/RC-ITER. Proceeding of the 5th International Symposium on Fusion Nuclear Technology (ISFNT-5), 19-24 September 1999, Rome, Italy. ITER Garching JCT

The first mirror of the system is located ~1 m behind the first wall in order to reduce the radiation loads and neutron streaming to the cover plate. The calculated specific nuclear heating here does not exceed ~ 20 mW/cm^3, the fast neutron flux ~ 5.6 x 10^{11} cm^{-2}s^{-1} and total neutron flux ~ 1.2 x 10^{12} cm^{-2}s^{-1}. This is by 2-3 orders of magnitude lower than at the first wall. Thus simple water-cooled, stainless steel mirrors can be used here.

Due to the "dog-leg" configuration, the neutron and photon fluxes attenuate along the channel by 5 orders of magnitude at the outlet lens. This does not change the average flux level inside the cryostat from that expected with a solid plug. Nuclear heat loads on the nearest cryogenic systems will not be disturbed by this diagnostic plug.

Another representative example is the combined LIDAR and polarimetry diagnostic system in the equatorial port (Figure 2.14-21) where the resulting streaming through the large channel (diameter 18-22 cm) might be a matter of concern.

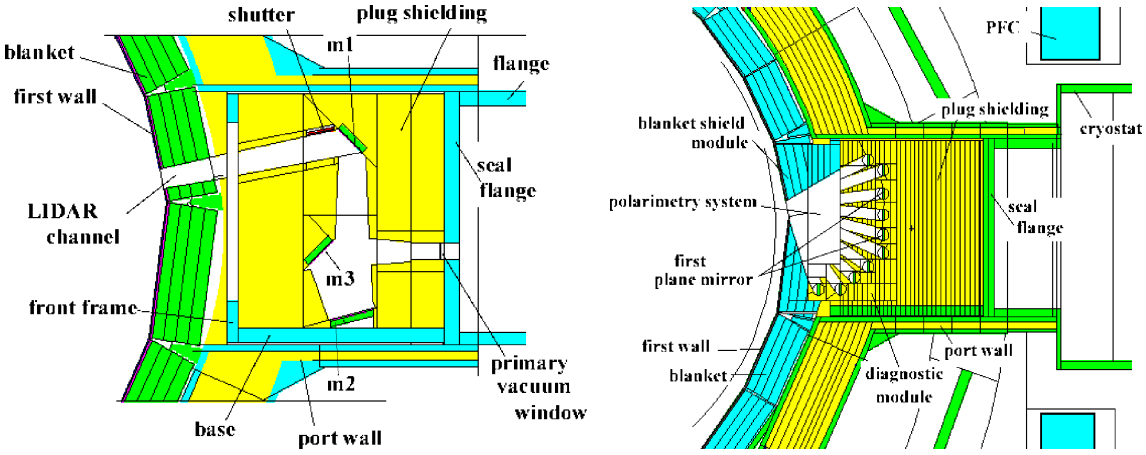

Figure 2.14-21 LIDAR and Polarimetry Diagnostic System Models for Nuclear Analysis

This streaming has in fact been evaluated to be acceptable adding only ~30% to the nearest PF3 and PF4 nuclear heating and to the neighbouring TF coil heating. Other limits for the magnet structure are also not exceeded.

The specific nuclear heating in the optical elements of the polarimetry system, which essentially consists of two fan-shaped vertical rows of 14 cm diameter angled tubes passing through a 23 x 14 cm aperture at the first wall, decreases from 50-150 mW/cm^3 in the mirrors to 1-7 µW/cm^3 in the quartz windows. The total neutron flux at the VV cover plate ("seal flange") surface is ~ 0.15-1 x 10^8 cm^{-2}s^{-1}. The residual dose rate between the seal flange and the cryostat due to neutron streaming throughout the diagnostic structure is below 80 µSv/h two weeks after shutdown. The total nuclear heat deposition in the diagnostic plug is ~ 2.9 MW which is a typical value for the blanket modules.

2.14.4.6 Dose Rate Outside Bioshield

2.14.4.6.1 Dose Rates from Irradiated Water Coolant Behind the Biological Shield

The outlet water coolant activated in the ITER plasma-facing regions is a source of high energy (~6 or 7 MeV) ^{16}N-decay photons and 0.9 MeV ^{17}N-decay neutrons ~ 1 minute after irradiation.

Operational dose rates at the outlet "hot" pipes outside the biological shield will be caused mainly by ^{16}N-decay photons. The estimated ^{16}N-specific activity in water here is ~1.3 x 10^9 Bq/cm^3. The corresponding absorbed dose rate is ~300 Gy/h at the pipe surface and ~5 Gy/h on the distance ~1 m from the pipe. Personnel access during operation in the outlet water pipe room, even behind the biological shield, is not allowed.

The ^{17}N-activity in water coolant is by 3 orders of magnitude lower than the ^{16}N-activity. The maximum expected residual dose rate initiated by the ^{17}N-decay neutrons at a steel pipe surface (0.10 wt% Co) is ~1.5-4 μSv/h two weeks after shut down, at the end of the first and the second decade of the DT operation campaign, respectively. This is several times lower than the expected corrosion product effects. The residual dose rates decrease rapidly, by 1-2 orders of magnitude at a distance ~ 0.5-1 m from the pipes.

2.14.4.6.2 Effect of Penetrations in Bio-shield

As mentioned previously, the bioshield has a thickness of 2 m and provides ~ 8 orders of magnitude attenuation during operation without considering penetrations. However, outside operation phases, assuming that the required 100 μSv/h is achieved in the cryostat, the bioshield only needs to produce one order of magnitude to reduce the dose rate to 10 μSv/h 10^6 s (~ 11 days) after shutdown. For places where more quick access (less than one day after shutdown) is required, two orders of magnitude reduction may be necessary, since dose rate at the shutdown is higher by ~ an order of magnitude than that 10^6 s after shutdown. There therefore seems to be plenty of margin in the bioshield to accommodate access after shutdown in the region outside it, providing penetration effects do not dominate.

Many penetrations are necessary to route hydraulic, electrical guides, etc. in the bioshield. Preliminary estimation shows that a hole with 50 cm radius provides an order of magnitude attenuation and that with 15 cm two orders of magnitudes. Most of the holes in the bio-shield have a radius less than 15 cm, for example the IC H&CD transmission line (R < 10 cm) and the EC H&CD waveguides (R < 10 cm).

In some cases, the size of penetration exceeds the above 15 cm or even 50 cm radius. As a typical case, penetrations for blanket cooling pipes have a 64 cm radius, including 36 cooling pipes. Proper shielding material should therefore be provided in the hole in order to give the required attenuation.

The above discussion assumes that the effect of concrete activation will be eliminated where it is necessary. This effect is important only when quick personnel access is required. Adding small amount of boron in the concrete, for example, will eliminate this effect.

2.14.5 The DD Phase Nuclear Performance

During the D phase preceding the DT phase, the DD (2.45 MeV) neutron yield ~ 3.5 x 10^{18} n/s will be accompanied by considerable tritium production. Assuming conservatively that all the generated tritium will react with the available deuterium, then a DT (14.1 MeV) neutron yield of ~ 3.5 x 10^{18} n/s is expected, leading to conditions which cannot be ignored from the radiation safety and maintenance standpoints.

The main nuclear characteristics of ITER, evaluated[1] for the two-component (2.45-MeV and 14.1-MeV) neutron source experienced in the proposed D operation phase, may be as high as: a high energy (> 0.1 MeV) neutron flux of ~ 2-4 x 10^{12} n/cm^{2}s, a neutron wall loading ~ 0.003-0.01 MW/m^2, and a first wall neutron fluence ~ 0.0006-0.002 MWa/m^2. These and other nuclear responses, are ~30-300 times lower than the values for the nominal DT-operation, depending on the tritium burn-up and gas removal (pumping) capability.

Taking into account the DD and DT neutron energy multiplication in the blanket (~ 4.2 and ~ 1.4 for the DD and DT neutrons), the secondary photon energy release and also the charged particle energy deposited in the plasma facing structures, a total nuclear power ~ 12-23 MW is estimated. (Auxiliary heating power of ~ 50-100 MW was not included in this value.)

Under this operation, the plasma chamber activation is three orders of magnitude lower than expected after the DT-phase. Nevertheless, personnel access to the plasma facing structures, such as the first wall and the divertor targets, will be restricted already after only a few tens of seconds of “full scale” DD-operations. At the same time the radiation conditions outside the machine behind the bulk radiation shield will allow for hands-on-maintenance almost immediately after reactor shutdown.

Thus, the foreseen DD-operation phase can be treated as an initial nuclear phase, and for this reason tritium production and removal, active cooling during the DD-plasma burn and after shut down, as well as remote handling of the in-vessel components, neutron diagnostics, and many ancillary systems, will need to be available from the very beginning of the DD-phase.

2.14.6 Conclusions

A fairly sophistcated nuclear analysis has been performed on ITER by means of the most detailed models and the best assessed nuclear data and codes. This has mainly been focused on:

- global and local nuclear heating for the component design;
- global and local shielding optimization;
- radiation conditions in different plasma heating and diagnostic systems;
- radiation conditions in and around the divertor port;
- activation of materials including the cooling water (see 5).

In the area of nuclear heating in the superconducting magnet system, the principal source is caused from neutrons and promptly emitted gamma rays. The total amount of TF coil heating

[1] V. Khripunov, Nuclear Performance of the D-D Phase of ITER, Proceeding of the 5th International Symposium on Fusion Nuclear Technology (ISNFT-5) 19-24 September 1999, Rome, Italy

has been computed to be less than 13 kW including the effect of shielding penetrations such as VV ports. The main contribution to this heating is localized in the inner leg of the magnet where the shielding has been optimized so as to reduce the overall radial build of the reactor. The volumetric local nuclear heating as well as the radiation damage to the copper and insulation materials of the magnet has been computed to be far below the respective limits.

In the light of the sufficiently thick blanket, helium production in the regions of required re-weldability in the vacuum vessel has also been evaluated to be within limits at the end of life.

Another important area of consideration, in view of its consequences for hands-on maintenance and unscheduled repairs, has been the dose rate for maintenance inside and outside the cryostat shell. In fact, neutrons do activate the reactor components during operation but, as a consequence of the presence of sufficient shielding, in most of the places the residual dose rate two weeks after shutdown is the level of the target for personnel access (100 μSv/h). Some local improvements have been identified to be required, in particular in the area around the NB system, and the shielding of the torus cryopumps, but no fundamental problems are foreseen.

In summary, the ITER nuclear response has been evaluated to be sound in all respects including magnet nuclear heating, radiation damage, activation, vessel helium production, etc. Further work in this area is needed to verify the local response of components still to be developed in full detail, such as port plugs and diagnostics systems.